Incubating Green Synthesized Iron Oxide Nanorods for Proteomics-Derived Motif Exploration: A Fusion to Deep Learning Oncogenesis

Yasmeen Manzoor, Murtaza Hasan,* Ayesha Zafar, Momina Dilshad, Muhammad Mahmood Ahmed, Tuba Tariq, Shahzad Gul Hassan, Shahbaz Gul Hassan, Aqeela Shaheen, Giovanni Caprioli,* and Xugang Shu*

Cite This: https://doi.org/10.1021/acsomega.2c05948

Read Online

| ACCESS | 📊 Metrics & More | 📖 Article Recommendations | 🖼 Supporting Information |

ABSTRACT: The nanotechnological arena has revolutionized the diagnostic efficacies by investigating the protein corona. This displays provoking proficiencies in determining biomarkers and diagnostic fingerprints for early detection and advanced therapeutics. The green synthesized iron oxide nanoparticles were prepared via *Withania coagulans* and were well characterized using UV−visible spectroscopy, X-ray diffraction analysis, Fourier transform infrared spectroscopy, and nano-LC mass spectrophotometry. Iron oxides were rod-shaped with an average size of 17.32 nm and have crystalline properties. The as-synthesized nanotool mediated firm nano biointeraction with the proteins in treatment with nine different cancers. The resultant of the proteome series was filtered oddly that highlighted the variant proteins within the differentially expressed proteins on behalf of nano-bioinformatics. Further magnification focused on S13_N, RS15, RAB, and 14_3_3 domains and few abundant motifs that aid scanning biomarkers. The entire set of variant proteins contracting to common proteins elucidates the underlining mechanical proteins that are marginally assessed using the robotic nanotechnology. Additionally, the iron rods indirectly possess a prognostic effect in manipulating expression of proteins through a smarter route. Thereby, such biologically designed nanotools provide a dual approach for medical studies.
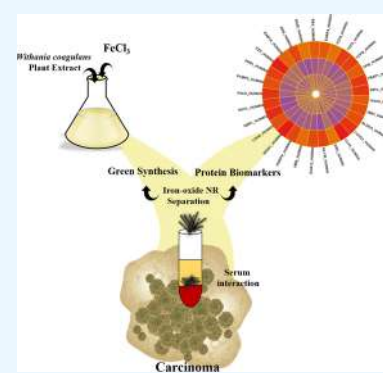
1. INTRODUCTION

On account of biomarker-based diagnostic trends, groundbreaking nanotechnological research studies are being performed for entangling, detecting, and operating biomarkers for advanced therapeutics.[1,2] The designing of functional nanoprobes ensures specific and stable targeting for harvesting biomarkers through biosystems in a more precise manner.[3,4] Among various nanotechnological probes, iron oxide nanoparticles are classified as biomedical materials that are significantly employed for life science studies.[5,6] Iron is very important due to its incredible superparamagnetic and biocompatible nature, showing significant results for magnetic resonance imaging,[7] targeted delivery of drugs,[8] proteins, nucleic acids, and antibodies for hyperthermia biosensing, tissue repair, and separation of biomolecules.[9−11] Furthermore, iron nanoparticles with different sizes, shapes, and high surface volume ratios that can also be controlled enhanced biomedical application results for challenging tasks.[12,13] Nanomaterials have encouraging physiochemical characteristics which have shown preclinical and clinical medical advances using iron oxide NPs for certain diagnostic probes.[14,15] Gold, zinc, copper, nickel, and SiO_2 have unique characteristics in biocompatibility, stability, surface area, size, morphology, and their interaction with the biological system, but iron nanoparticles possess excellent magnetic nature, high surface area,

and electrical and thermal conductivity. There are many ways to prepared novel and innovative nanoparticles with unique surface modification for multiple applications in the field of agriculture,[16] medical,[17] and different industries.[18] Physical and chemical methods are often applied for nanoparticle synthesis,[19,20] but due to the expensive mode, releasing hazardous chemicals and environmental degradation turn the researcher to switch on the biological method which is eco-friendly and biocompatible for the environment and living organism.[21,22] Green synthesis of nanomaterials is gaining more attraction due to being eco-friendly and having low-cost production, high stability, and biocompatibility. The addition of bioreducing agents via green chemistry methods has increased their wide range of physical and chemical characteristics for multiple application.[23−25] The biological routes govern definite shapes and sizes that provide increased surface area and also green chemistry to the designed particle[26] and further implicate higher interacting and catalytic domains for various applica-
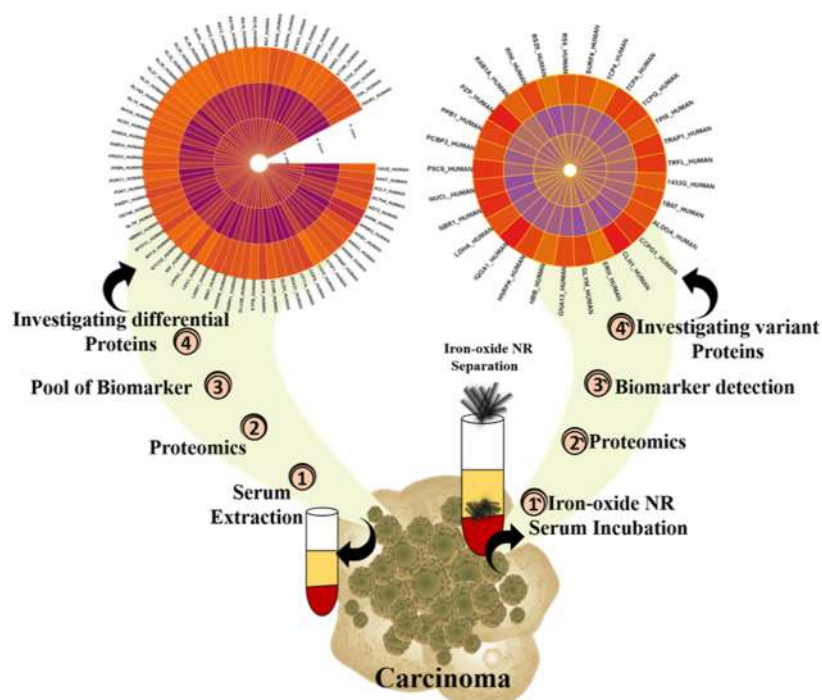
Figure 1. Schematic illustration of green synthesized iron oxide NRs and their incubation with different carcinoma serums for detection of variant proteins.

tion.[27] Taking advantage of iron NPs and their compatibility, various proteins have shown unique expression. Recently, multifunctional iron oxide magnetic nanoparticles have shown great success in biomarker detection, proteomic trails, and other biomedical applications. The iron oxide NPs form the protein corona due to higher compatibility with unique and specific oncogenic biomarkers.[28] Different sets of trials using green synthesized iron oxide NPs and various modification exhibited phenomenon results in biomarker detection and theragnostic.[29,30] Many researchers investigated the protein corona around nanoparticles for efficient detection of diseases at a very early stage for their proper treatment.[31,32] Previously, researchers found interesting results after incubating nanoparticles in various nutrient media for determination of their composition in the hard and soft corona.[33] In other studies, proteomics analysis of human serum was carried out after interaction of serum with silver, gold, and platinum nanoparticles to explore how the types of nanoparticles change the nature of protein interaction.[28,34] However, there is no documentation of data regarding the surface coating of natural biomolecules on the surface of nanoparticles for interaction and harvesting key and unique biomarkers. Interestingly, we aim to synthesize iron oxide NPs using the *Withania coagulans* extract that yields rod-shaped nanoparticles, detected through high-resolution microscopy analysis. In the next round, the green synthesized iron oxide NPs were treated with nine different cancerous serums (brain, breast, liver, muscles, neck, ovary, rectum, stomach, and testicular cancer) that were also examined under the microscopy technique for the conformation of the protein corona, where the most abundant carcinoma-treated particles were investigated through proteomics analysis techniques. Resultantly, the set of extracted oncogenic proteins were obtained and classified as common and differential proteins that were extracted using iron oxide NPs and serum-treated iron oxide NPs. This provided a pool

of biomarkers that directly and indirectly triggered oncogenic pathways. Here, we also emphasize the green chemistry as a responsive element in harvesting unique and hidden biomarkers.

2. RESULTS AND DISCUSSION

Cancer, being a kind of disease which kills hundreds of people everyday, demands for the introduction of new methods for early diagnosis at the very beginning stage.[35] For attaining this challenging task, current work was focused on green synthesis of the iron oxide nanostructure with the help of novel biomolecules acting as reducing agents from extracts of *W. coagulans*. This plant has already shown anticancer, hepatoprotective, anti-inflammatory,[36] antibacterial,[37] antiviral,[38] and reducing characteristics for the nanoparticle's synthesis.[39] The plant extract synthesized the Fe_2O_3 nanostructure by its reducing, capping, and antioxidant potentials that provided rod-shaped nanostructures. The nanorods (NRs) were characterized with the help of many latest techniques for the confirmation of their stability and underwent serum treatment of nine different carcinomas, as shown in the schematic in Figure 1. In the present study, iron oxide nanoparticles were synthesized using iron chloride as the precursor, and alpha-phase Fe_2O_3 of iron oxide was confirmed from the X-ray diffraction (XRD) pattern because all the peaks are well-matched with the alpha phase of Fe_2O_3. Different reports are available in which iron oxide nanoparticles were synthesized using iron chloride as a precursor.[40,41]

2.1. Incubation of Green Synthesized Iron Oxide NRs with Cancer Patient Serum and Their Characteristics. Plant *W. coagulans* was used as a reducing agent for preparing iron oxide NRs, as previously reported in our article.[42] These NRs were well characterized and were used as harvesters for variants proteins in the serum of cancer patients. Previously, it has been reported that the key biomarker and important
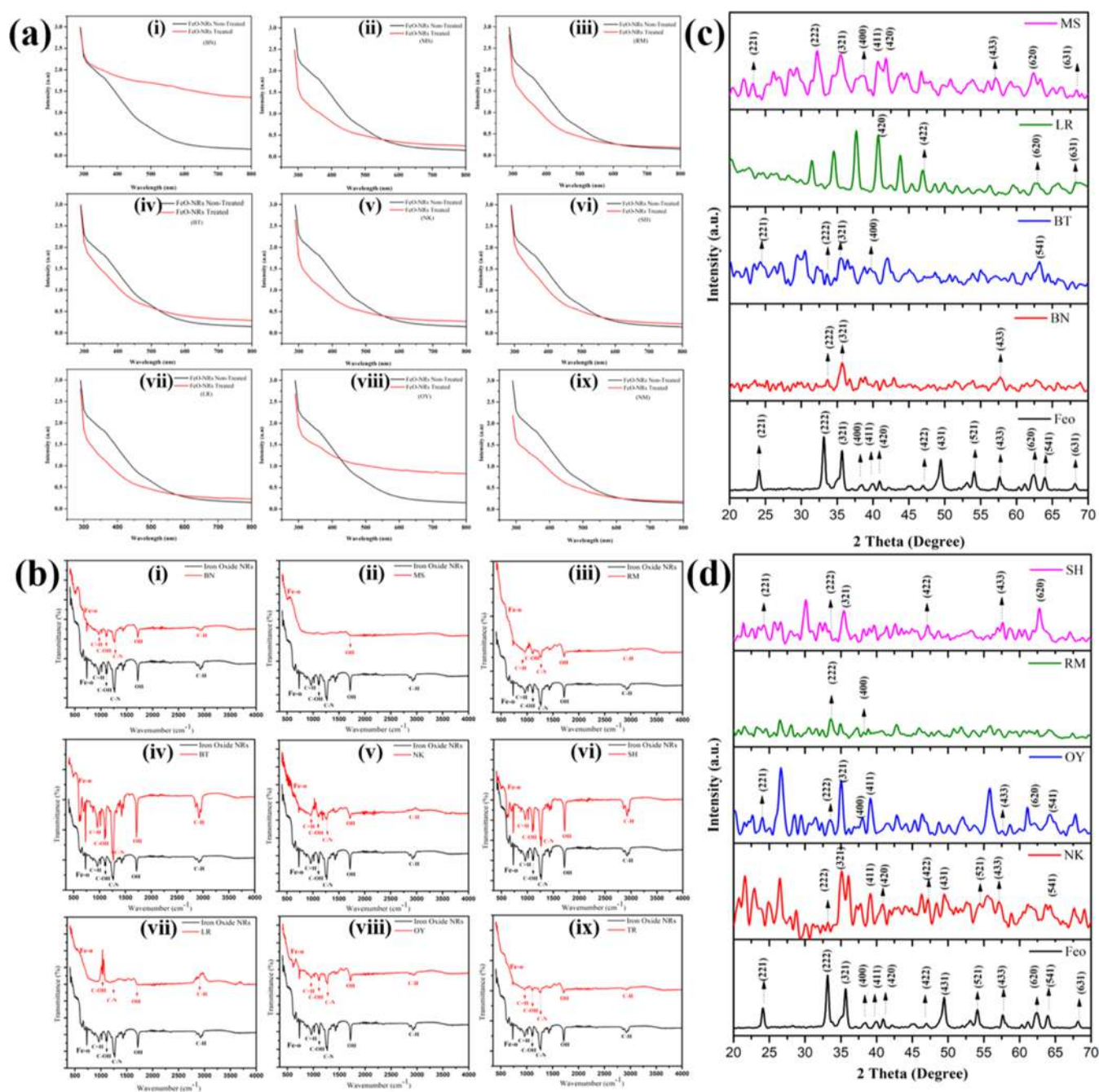
Figure 2. Characterization of iron oxide NRs after incubation with different cancer serums such as the brain (BN), breast (BT), liver (LI), muscles (MS), neck (NK), ovary (OY), rectum (RM), stomach (SH), and testicular cancer (TR). (a) UV−Vis spectra of iron oxide NRs before and after incubation with different cancer serums, (b) FT-IR analysis of iron oxide NRs before and after incubation with different cancer serums, (c) XRD analysis of incubated iron oxide NRs with cancer serum, and (d) XRD patterns of incubated iron oxide NRs with cancer serum.

secondary metabolites from the plants were harvested successfully.[43,44] Therefore, keeping in mind the efficient potential of nanotechnology, 300 mg of NRs in 1 mL of different cancer serums was incubated at 37 °C for 24 h for interaction and development of the protein corona. Later, the NRs with protein deposition were separated. The NRs with serum protein were ultracentrifuged at different speeds, revolutions, and time points to isolate the NRs from the supernatant. Finally, the serum-untreated iron oxide NRs and serum-treated iron oxide NRs were followed by different ultrafine techniques for characterization of NRs, proteomics profiling of the hard and soft corona, and bioinformatics

studies for interrogating the serum-interacted differentially expressed oncogenic biomarkers.

The very first ultraviolet (UV)-vis spectrometry provides prominent peaks at 360 nm in the visible region, which indicate the synthesized Fe_2O_3-NRs, whereas the serum-treated one shows peaks within 360−380 nm but with a lower intensity than the pure NP. The brain (BN) provides a peak at 315 nm [Figure 2a(i)], muscles (MS) provide a peak at 326 nm [Figure 2a(ii)], the rectum (RM) provides a peak at 361 nm [Figure 2a(iii)], the breast (BT) provides a peak at 326 nm [Figure 2a(iv)], the neck (NK) provides a peak at 374 nm [Figure 2a(v)], the stomach (SH) provides a peak at 374
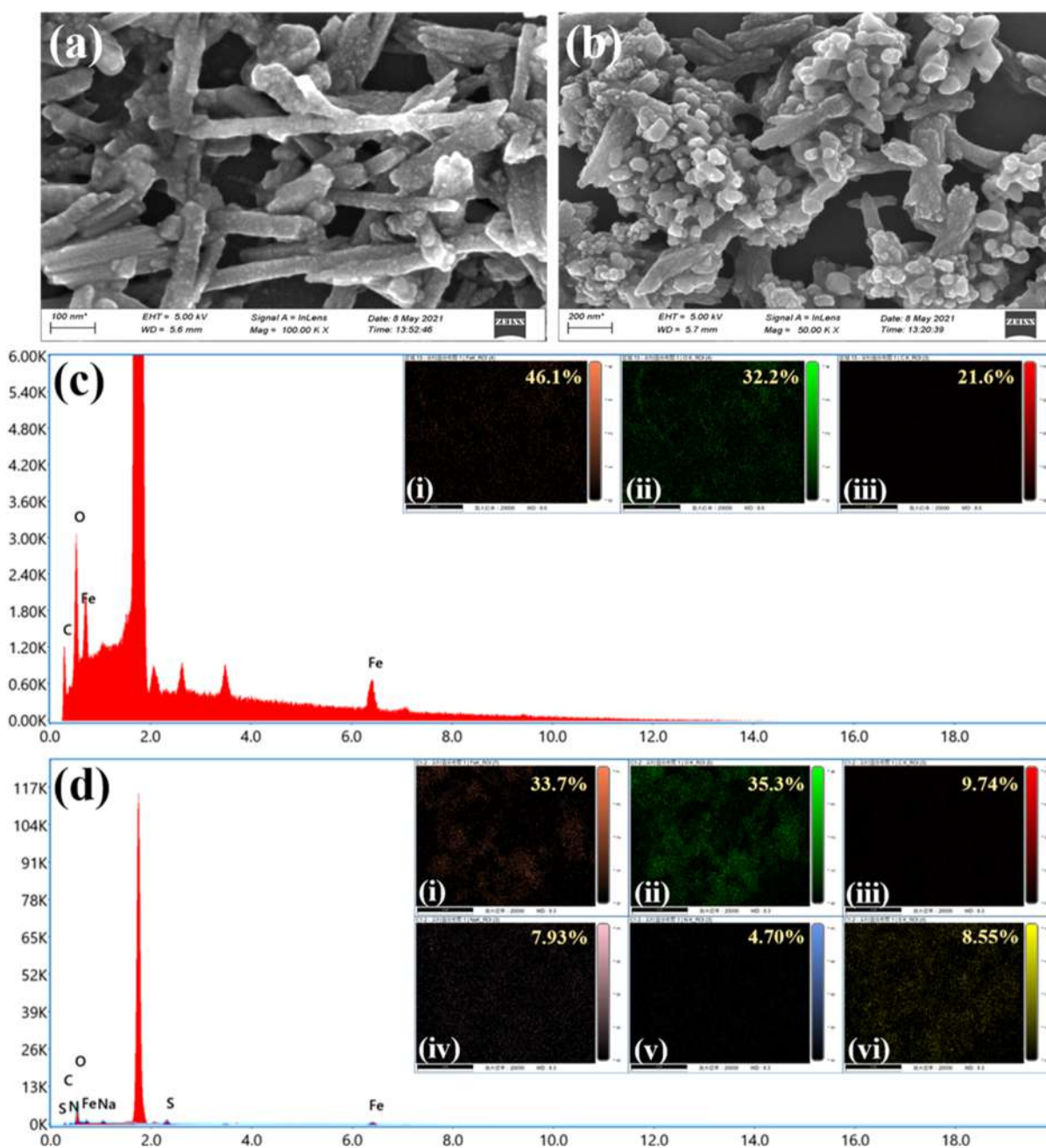
Figure 3. Scanning electron microscopy of iron oxide NRs before (a) and after (b) incubation with cancer serum and EDS of iron oxide NRs before (c) and after (d) incubation cancer serum.

nm [Figure 2a(vi)], the liver (LI) provides a peak at 374 nm [Figure 2a(vii)], the ovary (OY) provides a peak at 361 nm [Figure 2a(viii)], and the testicular (TR) provides a peak at 369 nm [Figure 2a(vix)]. The reason for the slight change in each case due to the addition is basically because of the corona developed onto the particles. The current studies show similar results to those previously reported about the formation of the corona on gold nanoparticles, which increased their stability against temperature.[45] In another work, UV results were very sensitive with nanoparticles and then the addition of albumin protein on it.[46] From the conclusion of previous results, we can say that the proteins coated on nanoparticles are sensitive for many biological assays and will be very useful for identification of markers in detection techniques. Fourier transform infrared spectroscopy (FT-IR) supported the green chemistry and

functional molecules of *W. coagulans* over the pure Fe_2O_3-NRs that include the characteristic peaks at 418, 637, and 733 cm^{-1} that belonged to the stretching vibration mode of iron oxygen (Fe_2O_3) bonds. 963 and 1017 cm^{-1} refer to C═H, 1108 cm^{-1} refers to C—OH, 1271 cm^{-1} represents the C—N bond, 1718 cm^{-1} represents the OH functional groups forming hydrogen bonds, and 2926 cm^{-1} shows C—H adsorption, whereas the treated FeO-NRs illustrated additional transmittance at 497, 1580 cm^{-1} for BN, as shown in [Figure 2b(i)], 497 and 1580 cm^{-1} for BT, as shown in [Figure 2b(iv)], 546, 1626, and 3690 cm^{-1} for LR, as mentioned in [Figure 2b(vii)], 509 and 1705 cm^{-1} for MS, as shown in [Figure 2b(ii)], 546, 1579, and 3693 cm^{-1} for NK, as shown in [Figure 2b(v)], 564 and 1585 cm^{-1} for OY, as shown in [Figure 2b(viii)], 1585 cm^{-1} for RM, as shown in [Figure 2b(iii)], 485 and 1579 cm^{-1} for SH, as
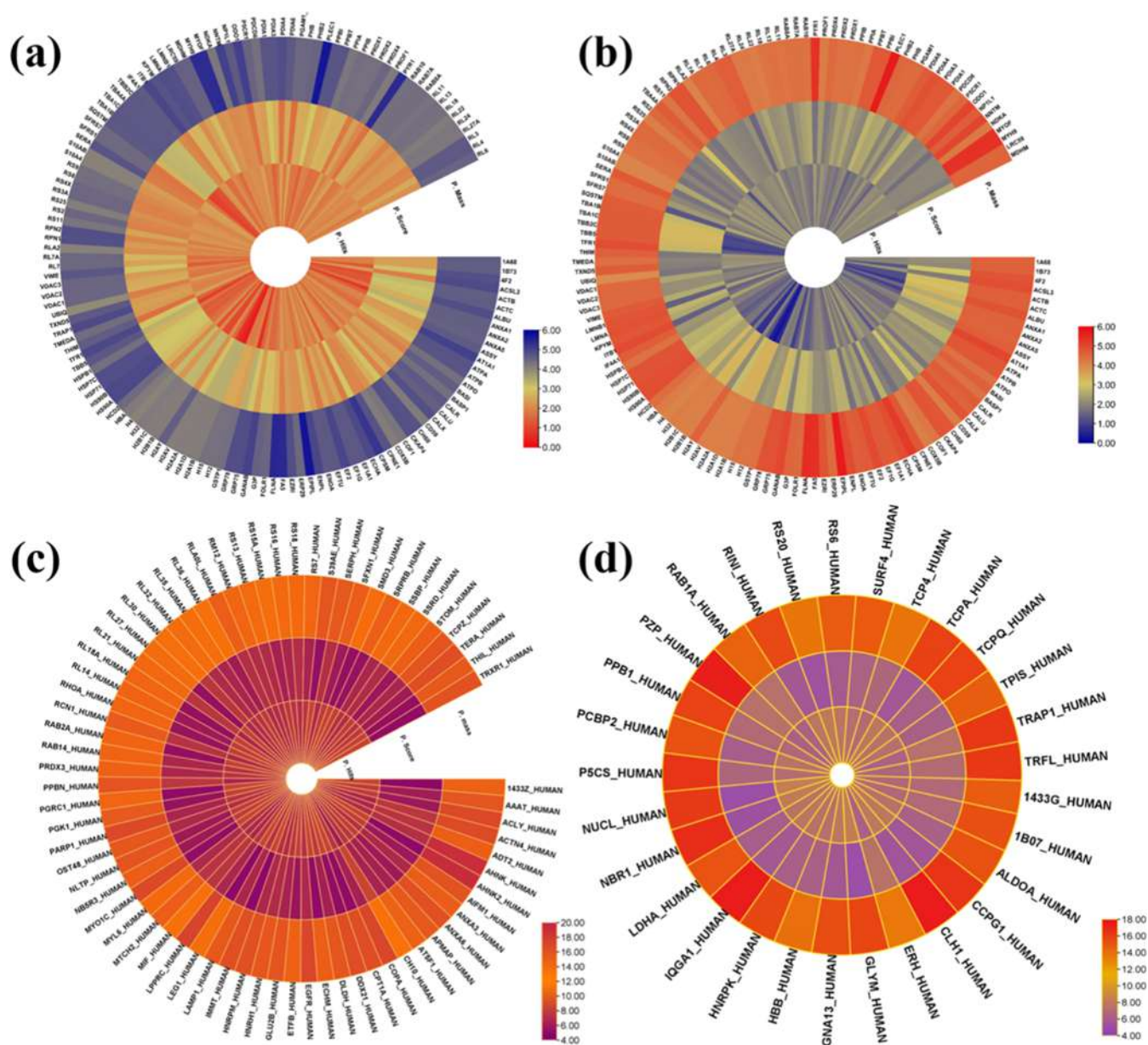
Figure 4. Differential expression of protein in cancer patient serum via iron oxide NRs. (a) Common protein in the untreated group. (b) Common protein in the treatment group. (c) Unique proteins in the untreated group. (d) Unique proteins in the treated group.

shown in [Figure 2b(vi)], and 606 and 1567 cm^{-1} for TR cancer, as mentioned in [Figure 2b(ix)].

These results show the attachment of different functional group on the surface of NRs, which confirmed the interaction of proteins having many amino acids resides on the nanoparticle surface. These results also give evidence and proof of already reported investigation on nanoparticles and protein corona.[47,48]

Next, the XRD analysis was carried out for further investigation for knowing the nature of NRs. X-rays Diffraction of pure Fe_2O_3-NRs having peaks at $2\theta = 24.17, 33.05, 35,71, 38.35, 40.00, 41.00, 47.05, 49.45, 52.00, 54.10, 57.63, 62.54, 64.12, 68.22$ corresponds to direction planes (211), (222), (321), (400), (411), (420), (422), (431), (521), (433), (620), (541), (631), respectively, as shown in Figure 2c (black), treated FeO-NRs that exhibited 33.05, 35.71, and 57.63 corresponds to the direction planes (222), (321), and (433), respectively, for BN, as shown in Figure 2c (red), 24.17, 33.05,

35.71, 38.35, and 64.12 correspond to the diffraction planes (211), (222), (321), (400), and (541) for BT, as mentioned in Figure 2c (blue), 41.00, 47.05, 62.54, and 68.22 correspond to direction planes (420), (422), (620), and (631) respectively, as shown in Figure 2c (green), for LI, 24.17, 33.05, 35,71, 38.35, 40.00, 41.00, 57.63, 62.54, and 68.22 correspond to direction planes (211), (222), (321), (400), (411), (420), (433), (620), and (631) respectively for MS, as shown in Figure 2c (purple), 33.05, 35,71, 40.00, 41.00, 47.05, 49.45, 54.10, 57.63, and 64.12 correspond to direction planes (222), (321), (411), (420), (422), (431), (521), (433), and (541), respectively, for NK, as shown in Figure 2d (red), 24.17, 33.05, 35.71, 38.35, 40.00, 57.63, 62.54, and 64.12 correspond to direction planes (211), (222), (321), (400), (411), (433), (620), and (541), respectively, for OY, as mentioned in Figure 2d (blue), 33.05 and 38.35 correspond to direction planes (222) and (400), respectively, for RM, as shown in Figure 2d (green), 24.17, 33.05, 35.71, 47.05, 57.63, and 62.54
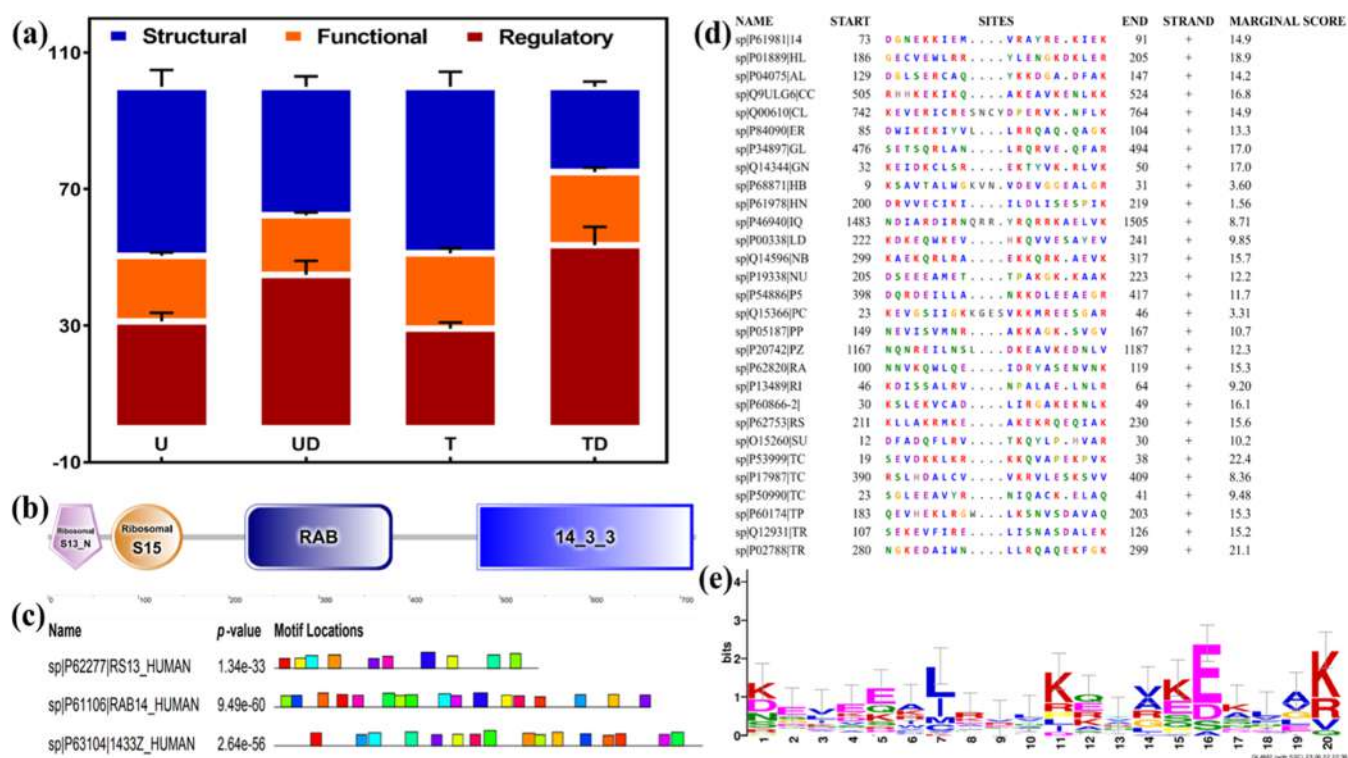
Figure 5. Functional analysis of variant proteins via bioinformatic tools (a), structural, functional, and regularity proteins (b), most abundant domains and motif structures (b,c), and variable length patterns and sequence logo (d,e).

correspond to direction planes (211), (222), (321), (422), (433), and (620), respectively, as shown for TR in Figure 2c,d (black). Changes in the structure of iron oxide NRs was observed carefully, and it was found that there were many granular changes due to the addition of proteomes or some metabolites which might be biomarkers for identification of cancer at an early stage. However, previously, it was reported that there was a significant difference in metabolite profiling with composition of the hard and soft corona around the nanoparticles.[49,50]

Furthermore, upon conducting examination, we have selected the breast, the most carcinoma, for further biomarker detection. For this, initially, we performed Scanning electron microscopy (SEM), which displayed rod-shaped structures with 17.32 nm size of iron and aggregated proteins over the Fe_2O_3-NRs in the treatment group, Figure 3a,b. Furthermore, energy-dispersive X-ray spectroscopy (EDS) elucidated the green chemistry over the pure Fe_2O_3-NRs with percentages of 46.1, 32.2, and 21.6% for iron, oxygen, and carbon, respectively, and protein functional groups over the serum-treated groups as iron, oxygen, carbon, sodium, nitrogen, and sulfur with percentages of 33.7, 35.3, 9.74, 7.93, 4.70, and 8.55%, respectively, Figure 3c,d. Over to the characterization, the Fe_2O_3-NRs and the particles were channeled for the proteomics over the serum control and protein corona over the treated Fe_2O_3-NRs. After careful observation and comparisons with previous results, we can conclude that there is strong interaction between cancer serum the proteomics biomarker with NRs for making distinction of nanoparticle characteristics of incubated and non-incubated nanoparticles.[51,52]

2.2. Proteomics Analysis of Cancer Patient Serum in Response to Iron Oxide NR Incubation. The study initially investigated the characteristic property of the particle and the proteins inside the serum specifically. The cascade of

characterization provides satisfactory results for compatibility and protein deposition. However, due to the lack of blood serum (due to less amount of blood in patients, availability, study layout, sample handling, etc.), we pointed out the most occurring cancer of the survey region so that we hybridize nanotechnology, proteomics, and bioinformatics deep learning that can highlight key biomarkers. Thereby, breast cancer provided a huge number of biomarkers and considered the more abundant cancer form through previous studies, whereas the obtained biomarkers were the major reason for causing breast cancer. The selected cancer provided with wide range of biomarkers for diagnosis and nano-prognosis. The control group provided with 210 biomarker proteins, Figure 4a, whereas the treated group provided with 169 oncogenic proteins that are mostly reported, as shown in Figure 4b. These differential-expressed oncogenic proteins were further elucidated and classified into common and unique proteins, where the untreated UT provided 140 common and 70 unique proteins, as shown in Figure 4c, and the treated group successfully captured 29 variant classes of proteins along with 140 common proteins, as shown in Figure 4d. These sets of common proteins are already reported.[53] In order to scavenge underlining oncogenic proteins, motifs, and domains common, a nanoprobe was introduced.

The nanoprobe being biocompatible and enduring green surface chemistry scavenges the far-located responsive proteins.[54] The classical role of these oncogenic protein biomarkers was interrogated using bioinformatics tools for tracing back and forth of the protein function, motifs, and domains.[55] The variant class of untreated and treated groups was analyzed through bioinformatics screening provided with multifunctional and regulatory roles of protein that primes the JAK-STAK and FOS-JUN pathway, affecting the translational and metastatic pathway. Therefore, the innovative green

synthesized rod-shaped Fe_2O_3-NRs aid in efficient detection of oncogenic markers.[56,57]

2.3. Functional Analysis of Variant Protein via Bioinformatic Tools.

Functional aspects were revealed for untreated (U), untreated differential (UD), treated (T), and treated differential (TD) sets of proteins through exploring functional annotations based on ortholog assignments and domain prediction. The output categorized the four sets of proteins into structural, functional, and regulatory proteins, and interestingly, both differential sets of proteins (UD and TD) were accumulated with a greater number of regulatory proteins and relatively a smaller number of structural proteins as compared to other two (U and T) sets of proteins (Figure 5a). The highest number of regulatory proteins were observed for TD; hence, it was emphasized for downline bioinformatics explorations (Figure 5a). To further explore the structural aspects, the most abundant domains and motif structures were identified and visualized for TD (Figure 5b,c). Among the most recurring protein domains, ribosomal_S13_N and ribosomal_15 are structural constituents of ribosomes which involved in the cellular metabolic process of protein synthesis. Likewise, RAB (guanosine triphosphatases) and 14-3-3 (epsilon) domain harboring proteins are involved in transportation and molecular signaling across the membrane at the cellular level. Proteins containing these domains have shown to mediate the cellular metabolic processes in the stimulus to carcinoma stress factors at the cellular level. Similarly, motif patterns in these recurring proteins were found variable, showing a degree of variability in these protein domains (Figure 5c). Furthermore, to explore the recurring variable length patterns in 29 proteins of the TD set, the most conserved motif pattern was identified and visualized as the sequence logo (Figure 5d,e). The results depicted the existence of a marginally conserved short motif (20 aa) at different positions among TD set proteins. Overall, these findings persuaded that the TD set of proteins accumulated novel proteins with peculiar characteristics, and this set could aid in for the diagnosis of diseases. Knowing the structure, functionality, and regularity of proteins, the current work can predict the important biomarkers for the detection of diseases at the early stage.[58,59]

The set of obtained proteins that were found common and differential are considered to be the significant biomarkers for multiple carcinomas that include HBB,[60] GNA13,[61] enhancer of the rudimentary homologue,[62,63] CCPG1, ALDOA, TRFL, TRP1, RAB1A, Ras-related protein Rab-7a, RPL21 60S ribosomal protein L21, ACTC1, ribosomal protein S25, Ras-related protein Rab-8A, heat shock protein HSP 90-beta,[64,65] beta-subunit of prolyl 4-hydroxylase (P4HB), carbamoyl phosphate synthetase I, pyrroline-5-carboxylate reductase 1, and so forth.[66,67] The resultant proteins are differentially expressed and captured by a single probe that has multiple binding and capturing sites. The green surface chemistry provides surface enhancement using biomolecules that provide more attachment sites. This majorly contributes to oxidative stress, metabolic stress, and activation of oncogenic pathways that generate tumor progression. Therefore, blueprinting these biomarkers using a single probe facilitates in capturing and identifying biomarkers for early detection. Advance materials have shown enhanced efficacies in detecting and prognosis of various carcinomas.

3. EXPERIMENTAL SECTION

3.1. W. coagulans Extract Preparation.
Cordia myxa plants were obtained from the local area of Bahawalpur, Pakistan. The whole plant was thoroughly washed with tap water to remove dirt and then washed with distilled water. The fruits of *W. coagulans* were washed, dried, and ground finely. Powder (10 g) was added in 100 mL of distilled water and kept for boiling at 90 °C for nearly 50 min. The heated mixture was filtered using Whatman filter paper and then stored at 4 °C.

3.2. Preparation of Iron Oxide NRs and Characterization.
The synthesis of iron oxide NPs was performed by adding $FeCl_3 \cdot 6H_2O$ and $FeCl_2 \cdot 4H_2O$ (1:2 molar ratios) in 100 mL of double distilled water in a 250 mL reagent bottle. The mixture was heated and stirred at 80 °C using the magnetic stirrer for 1 min. After this, 20 mL of aqueous solution of the *W. coagulans* plant extract (used as a reducing agents) was added to the mixture. After 15 min, 20 mL of aqueous solution of sodium hydroxide (for maintaining the pH of solution) was added with the ratio of 3 ml per minute, and a change in color was observed. The iron oxide NPs precipitated uniformly, and they were allowed to cool at room temperature. After 30 min, iron oxide NRs were obtained by decanting and followed by three times washing with distilled water and one time with ethanol and later dried in an oven to obtain the powder of iron oxide NRs.

3.3. Collection of the Blood Sample.
The next round after synthesizing iron oxide NRs was serum treatment with iron oxide NRs, their separation, and proteomics analysis. For this, ethical approval was signed by the institutional review board committee of biotechnology department of Islamia University of Bahawalpur, Pakistan. The collection of blood from different cancer patients was carried out in the Bahawal Victoria Hospital Bahawalpur, Pakistan. All of the case samples (patients) were admitted in the different wards of the hospital. Before collection of the sample, concerns of the patient and their family were noted, and also, the questioners that contain the patient history (S1) was filled and signed. The blood was collected in the ethylene diaminetetraacetic acid (EDTA)-coated (BOLTON Scientific Limited) vile with a total collection capacity of 4 mL. The collected blood samples were put in the dry ice box and safely taken to the departmental laboratory.

3.4. Serum Separation from Blood.
In the laboratory, the serum was separated from the blood immediately after the collection of blood. After the separation of serum from all blood samples of different cancer patients, the author has divided cancer patients' serum into different groups according to the cancer type. The author has divided serum samples into nine different types of cancers, such as brain cancer, breast cancer, liver cancer, stomach cancer, muscles cancer, testicular cancer, ovary cancer, neck cancer, and rectum cancer. Now, these nine different types of cancer serum groups were divided into two parts. 50% of serum of all cancer types was separated for interaction with iron oxide NRs; then, characterization and protein profiling were carried out, and other 50% was used for protein profiling without interaction with iron oxide NRs.

3.5. Interaction of Serum with Iron Oxide NRs.
All nine different groups of cancer serums were incubated with iron oxide NRs for 24 h. NRs (300 mg) were added in 1 mL of cancer serum of breast cancer. Now, this sample was placed in an incubator at 37° for 24 h. Similarly, all nine types of cancer serums were interacted with iron oxide NRs separately

following this procedure. Also, this procedure was repeated until all serums were treated.

3.6. Iron Oxide NR Separation after Incubation Periods. After the completion of the incubation period, separation of iron oxide NRs and serum was carried out. Samples were put into a centrifuge machine, and they were centrifuged at 10,000 rpm for 5 mints. After 5 min centrifugation, the NRs were settled down at the bottom, and serum was present at the upper side as a supernatant. The serum of each different type was separated into separate labeled falcon tubes. Now, iron oxide NRs in the bottom were washed three times with distilled water and one time with ethanol and also separated out and were placed in an incubator at 70 for 15 min. All nine groups of cancer serum after interaction with iron oxide NRs were stored at −30 °C for proteomics, and the serum-treated dried iron oxide NRs were ground into fine powder and stored in the separated labeled Eppendorf tubes and were used further for characterization.

3.7. UV−Vis Spectrophotometry. Analysis of iron oxide NRs incubated with cancer patient serum was caried out using ultraviolet spectrometry. In this technique, iron NRs coated with proteins from serum were monitored using periodic sampling of aliquots, and time by time spectra of the solution were measured. These spectra were recorded after every 30 min, and the UV spectrum of all aliquots was monitored as a function of time retention on the UV spectrophotometer operated at a resolution of 1 nm.

3.8. XRD Analysis. The diffracted intensities of the air-dried samples of Fe_2O_3-NRs with serum of cancer patients were recorded to determine the crystal structure and size of the nanoparticles using XRD spectroscopy (Rigaku, Ultima IV, X-ray diffractometer system). Using Cu Kα ration voltage, all diffracted intensities were recorded at 40 KV and 30 mA current in the 20−80 scanning range.

3.9. Fourier-Transform Infrared Spectroscopy. The FT-IR analysis was carried out for the attachment of functional groups on Fe_2O_3-NRs with the capping agent. Air-dried iron oxide NPs are converted into pellets, and at a resolution of 4 cm^{-1} and in a range of 50−3500 cm^{-1}, FT-IR analysis was carried out using a Thermo Scientific spectrophotometer.

3.10. Scanning Electron Microscopy. The morphology, texture, and elemental composition of serum-induced Fe_2O_3-NRs were studied using a Quanta Inspect scanning electron microscope, operating at 25 kV in vacuum. For this purpose, iron oxide NRs were used in the powder form.

3.11. Proteomics Analysis. Cancer serum was treated with 300 mg of iron oxide NRs for 24 h. The serum containing proteins was adhered on the surface of NRs during incubation time. After the time point, trypsin was used to eradicate the protein corona present on NRs. For purification and removal of debris, 0.5 mL of isoelectric focusing buffer with 30 mM Tris, 3 M urea (5 mL), 1 M thiourea (5 mL), 2% 3-[(3-cholamidopropyl) dimethylammonio]-1-propanesulfonate (15 mL), 5 mM 1−4 dithioerythritol, and 0.5 mM EDTA was used. This decontaminated nanocomplex was centrifuged at 3000 rpm for an hour at 4 °C. Finally, separated protein content was finally measured using the Bradford reagent.

Extracted proteins from the NRs incubated in cancer serum were initially denatured by 50 μL of 6 M urea and then with 6 μL of 100 mM 2.2-dithiodipyridine (DTP) which lyophilized with 6 h incubation at 37 °C.[68,69] The samples were then kept in the alkaline environment by adding 30 μL of 100 mM iodocamide for 24 h in the dark. Finally, adding 600 u L of 50

mM NH_4CO_3 (pH 8.2) and 40 μL of trypsin (0.5 mg/mL) results in the formation of peptides and continued for 20 h at room temperature. The protein samples were added to at a flow rate of 0.5 mL/min to the 250 mm column under set conditions according to Agilent 300 A SCX 4.6 mm. The mobile phase of solvent (A) consisted of 15 mM ammonia format and 25% acetonitrile at pH of 3, while solvent (B) was composed of 500 mM ammonium format and 25% acetonitrile at a pH of 6.8. A 3−4% linear gradient of B separated peptides over 50 min at 280 nm. The fractions of protein peptides were collected after every 2 min and stored at 80 C. The column C18 (Column Technology Inc., Fremont, CA, USA) was used to elute the samples with a linear acetonitrile gradient elution from 100% solvent for liquid chromatography−mass spectrometry (MS)/MS analysis or Agilent electrospray−ion trap (ESI-Trap) mass spectrometry analysis.[70,71] Both solvent A consisting of the 70% water-based mixture with 0.1% formic acid and solvent B consisting of the 30% acetonitrile-based mixture with 0.1% formic acid were kept in the column for 2 h with a flow rate of 2.01 mL/min. When operating ESI−TOF and ESI−TROP analyzers, the nebulizer pressure was kept at 25 psi. The drying gas (nitrogen) flow was 12 mL/min with a temperature of 310 °C.

3.12. Bioinformatic Analysis. Swissprot peptide identifiers were used to extract FASTA sequences, and orthology assignments using precomputed phylogenetic cluster-based functional annotation was performed using eggnog-mapper v2.[72] The GO terms were parsed through a built-in package in TBtools,[73] and the outcome aided in predicting three kinds of proteins, that is, structural, functional, and regulatory ones. Domains of the most redundant proteins among the four treatments were visualized using the CDD tool,[74] while the gapped local motif alignment was scanned through calling the GLAM2 function in the MEME suite.[75]

4. CONCLUSIONS

In conclusion, Fe_2O_3-NRs were synthesized by the green method using the *W. Coagulans* as the effective reducing and stabilizing agent. The synthesized particles were bifurcated into pure Fe_2O_3-NRs and oncogenic serum-treated Fe_2O_3-NRs with nine different cancers. The first series included synthesis and characterization of both groups and later blueprinting the oncogenic protein biomarker through proteomics. This elucidated 30 common and 25 differential biomarkers using the green Fe_2O_3-nanoprobe. The biomolecules provide an additional binding site for obtaining a pool of oncogenic biomarkers, whereas the bioinformatics algorithm provides a precise range of biomarkers. The metallic probe highlights the most significant and abundant biomarkers using the biologically decorated probe. This proved the advance and unique nanotechnological arena for harvesting the least detected and specific biomarker in a more sophisticated way.

■ ASSOCIATED CONTENT

ⓢ Supporting Information

The Supporting Information is available free of charge at https://pubs.acs.org/doi/10.1021/acsomega.2c05948.

Questionnaire regarding patient history (PDF)

◾ AUTHOR INFORMATION

Corresponding Authors

Murtaza Hasan − *Department of Biotechnology, The Institute of Biochemistry, Biotechnology and Bioinformatics, The Islamia University of Bahawalpur, Bahawalpur 63100, Pakistan; College of Chemistry and Chemical Engineering, Zhongkai Agriculture University and Engineering Guangzhou, Guangzhou 510225, PR China;* ⓘ orcid.org/ 0000-0001-7715-9173; Email: murtaza@zhku.edu.cn; Fax: 92-346-7578898

Giovanni Caprioli − *Chemistry Interdisciplinary Project (CHip), School of Pharmacy, University of Camerino, Camerino 62032, Italy;* ⓘ orcid.org/0000-0002-5530-877X; Email: giovanni.caprioli@unicam.it

Xugang Shu − *College of Chemistry and Chemical Engineering, Zhongkai Agriculture University and Engineering Guangzhou, Guangzhou 510225, PR China;* ⓘ orcid.org/0000-0002-0613-5083; Email: xgshu@ 21cn.com

Authors

Yasmeen Manzoor − *Department of Biotechnology, The Institute of Biochemistry, Biotechnology and Bioinformatics, The Islamia University of Bahawalpur, Bahawalpur 63100, Pakistan*

Ayesha Zafar − *Department of Biotechnology, The Institute of Biochemistry, Biotechnology and Bioinformatics, The Islamia University of Bahawalpur, Bahawalpur 63100, Pakistan; Department of Biomedical Engineering, College of Future Technology, Peking University, Beijing 510225, PR China*

Momina Dilshad − *Department of Biotechnology, The Institute of Biochemistry, Biotechnology and Bioinformatics, The Islamia University of Bahawalpur, Bahawalpur 63100, Pakistan*

Muhammad Mahmood Ahmed − *Department of Bioinformatics, The Institute of Biochemistry, Biotechnology and Bioinformatics, The Islamia University of Bahawalpur, Bahawalpur 63100, Pakistan*

Tuba Tariq − *Department of Biotechnology, The Institute of Biochemistry, Biotechnology and Bioinformatics, The Islamia University of Bahawalpur, Bahawalpur 63100, Pakistan*

Shahzad Gul Hassan − *National Institute of Cardiovascular Diseases (NICVD) Cantonment, Karachi 75510, Pakistan*

Shahbaz Gul Hassan − *College of Information Science and Engineering, Zhongkai University of Agriculture and Engineering, Guangzhou 510225, China*

Aqeela Shaheen − *Deaprtment of Chemistry, Govt, Sadiq College Women University, Bahawalpur 63100, Pakistan*

Complete contact information is available at:
https://pubs.acs.org/10.1021/acsomega.2c05948

Notes

The authors declare no competing financial interest.
The Islamia University of Bahawalpur and Bahwal Victoria Hospital animal care and human rights committee approved all the experimental procedure and laboratory protocol used for this study (Protocol # 2012A).

◾ REFERENCES

(1) Napione, L. Integrated Nanomaterials and Nanotechnologies in Lateral Flow Tests for Personalized Medicine Applications. *Nanomaterials* **2021**, *11*, 2362.

(2) Hasan, M.; Gulzar, H.; Zafar, A.; ul Haq, A.; Mustafa, G.; Tariq, T.; Khalid, A.; Mahmmod, A.; Shu, X.; Mahmood, N. Multiplexing Surface Anchored Functionalized Iron Carbide Nanoparticle: A Low Molecular Weight Proteome Responsive Nano-Tracer. *Colloids Surf., B* **2021**, *203*, 111746.

(3) Hasan, M.; Mustafa, G.; Iqbal, J.; Ashfaq, M.; Mahmood, N. Quantitative Proteomic Analysis of HeLa Cells in Response to Biocompatible Fe2C@C Nanoparticles: 16O/18O-Labelling & HPLC-ESI-Orbit-Trap Profiling Approach. *Toxicol. Res.* **2018**, *7*, 84−92.

(4) Hasan, M.; Yang, W.; Ju, Y.; Chu, X.; Wang, Y.; Deng, Y.; Mahmood, N.; Hou, Y. Biocompatibility of Iron Carbide and Detection of Metals Ions Signaling Proteomic Analysis via HPLC/ ESI-Orbitrap. *Nano Res.* **2017**, *10*, 1912−1923.

(5) Khan, S.; Akhtar, N.; Ur Rehman, S.; Shujah, S.; Rha, E. S.; Jamil, M. Biosynthesized Iron Oxide Nanoparticles (Fe3o4 Nps) Mitigate Arsenic Toxicity in Rice Seedlings. *Toxics* **2021**, *9*, 2.

(6) Archana, S. A Comparative Study of Iron Oxide Nanoparticles Surface Modified Using Carboxylic Acids. *Int. J. Res. Appl. Sci. Eng. Technol.* **2021**, *8*, 13.

(7) Volokhova, M.; Shugai, A.; Tsujimoto, M.; Kubo, A. L.; Telliskivi, S.; Nigul, M.; Uudeküll, P.; Vija, H.; Bondarenko, O. M.; Adamson, J.; Kahru, A.; Stern, R.; Seinberg, L. Cubic Iron Core−Shell Nanoparticles Functionalized to Obtain High-Performance MRI Contrast Agents. *Materials* **2022**, *15*, 2228.

(8) Du, H.; Akakuru, C. Y.; Yao, H.; Yang, B.; Wu, S. X.; Yao, J. L.; Zheng, F.; Yang, F.; Wu, A. G. Applications of Transition Metal-doped Iron-based Nanoparticles in Biomedicine. *Chin. J. Appl. Chem.* **2022**, *15*, 101264.

(9) Boss, A.; Heeb, L.; Vats, D.; Starsich, F. H. L.; Balfourier, A.; Herrmann, I. K.; Gupta, A. Assessment of Iron Nanoparticle Distribution in Mouse Models Using Ultrashort-Echo-Time MRI. *NMR Biomed.* **2022**, *35*, 4690.

(10) Selzer, S. M.; Vico, R. v.; Ferreyra, N. F. Immobilization of Concanavalin A on Iron Oxide Magnetic Nanoparticles. Effect of Bovine Serum Albumin in the Recognition Interactions of the Lectin. *Surface. Interfac.* **2022**, *30*, 101908.

(11) Covarrubias-Zambrano, O.; Motamedi, M.; Ameredes, B. T.; Tian, B.; Calhoun, W. J.; Zhao, Y.; Brasier, A. R.; Kalubowilage, M.; Malalasekera, A. P.; Yapa, A. S.; Wang, H.; Culbertson, C. T.; Troyer, D. L.; Bossmann, S. H. Optical Biosensing of Markers of Mucosal Inflammation. *Nanomedicine* **2022**, *40*, 102476.

(12) Hussain, M. H.; Abu Bakar, N. F.; Mustapa, A. N.; Low, K. F.; Othman, N. H.; Adam, F. Synthesis of Various Size Gold Nanoparticles by Chemical Reduction Method with Different Solvent Polarity. *Nanoscale Res. Lett.* **2020**, *15*, 140.

(13) Shamhari, N. M.; Wee, B. S.; Chin, S. F.; Kok, K. Y. Synthesis and Characterization of Zinc Oxide Nanoparticles with Small Particle Size Distribution. *Acta Chim. Slov.* **2018**, *65*, 578−585.

(14) Qasim, S.; Zafar, A.; Saif, M. S.; Ali, Z.; Nazar, M.; Waqas, M.; Haq, A. U.; Tariq, T.; Hassan, S. G.; Iqbal, F.; Shu, X. G.; Hasan, M. Green Synthesis of Iron Oxide Nanorods Using Withania Coagulans Extract Improved Photocatalytic Degradation and Antimicrobial Activity. *J. Photochem. Photobiol., B* **2020**, *204*, 111784.

(15) Mahdavi, M.; Namvar, F.; Ahmad, M.; Mohamad, R. Green Biosynthesis and Characterization of Magnetic Iron Oxide (Fe 3O4) Nanoparticles Using Seaweed (Sargassum Muticum) Aqueous Extract. *Molecules* **2013**, *18*, 5945.

(16) Hasan, M.; Rafique, S.; Zafar, A.; Loomba, S.; Khan, R.; Hassan, S. G.; Khan, M. W.; Zahra, S.; Zia, M.; Mustafa, G.; Shu, X.; Ihsan, Z.; Mahmood, N. Physiological and Anti-Oxidative Response of Biologically and Chemically Synthesized Iron Oxide: Zea Mays a Case Study. *Heliyon* **2020**, *6*, 04595.

(17) Sarkar, T.; Bharadwaj, K. K.; Salauddin, M.; Pati, S.; Chakraborty, R. Phytochemical Characterization, Antioxidant, Anti-Inflammatory, Anti-Diabetic Properties, Molecular Docking, Pharma-cokinetic Profiling, and Network Pharmacology Analysis of the Major Phytoconstituents of Raw and Differently Dried Mangifera Indica (Himsagar Cultivar): An In Vitro and In Silico Investigations. *Appl. Biochem. Biotechnol.* **2022**, *194*, 950−987.

(18) Ribeiro, A. S.; Costa, S. M.; Ferreira, D. P.; Calhelha, R. C.; Barros, L.; Stojković, D.; Soković, M.; Ferreira, I. C. F. R.; Fangueiro, R. Chitosan/Nanocellulose Electrospun Fibers with Enhanced Antibacterial and Antifungal Activity for Wound Dressing Applica-tions. *React. Funct. Polym.* **2021**, *159*, 104808.

(19) Reverberi, A. P.; Kuznetsov, N. T.; Meshalkin, V. P.; Salerno, M.; Fabiano, B. Systematical Analysis of Chemical Methods in Metal Nanoparticles Synthesis. *Theor. Found. Chem. Eng.* **2016**, *50*, 59−66.

(20) Satyanarayana, T. A. Review on Chemical and Physical Synthesis Methods of Nanomaterials. *Int. J. Res. Appl. Sci. Eng. Technol.* **2018**, *6*, 2885−2889.

(21) Hasan, M.; Ullah, I.; Zulfiqar, H.; Naeem, K.; Iqbal, A.; Gul, H.; Ashfaq, M.; Mahmood, N. Biological Entities as Chemical Reactors for Synthesis of Nanomaterials: Progress, Challenges and Future Perspective. *Mater. Today Chem.* **2018**, *8*, 13−28.

(22) Vigneswari, S.; Amelia, T. S. M.; Hazwan, M. H.; Mouriya, G. K.; Bhubalan, K.; Amirul, A. A. A.; Ramakrishna, S. Transformation of Biowaste for Medical Applications: Incorporation of Biologically Derived Silver Nanoparticles as Antimicrobial Coating. *Antibiotics* **2021**, *10*, 229.

(23) Zulfiqar, H.; Zafar, A.; Rasheed, M. N.; Ali, Z.; Mehmood, K.; Mazher, A.; Hasan, M.; Mahmood, N. Synthesis of Silver Nano-particles Using: Fagonia Cretica and Their Antimicrobial Activities. *Nanoscale Adv.* **2019**, *1*, 1707−1713.

(24) Hasan, M.; Altaf, M.; Zafar, A.; Ali, Z.; Munawar, T.; Saif, M. S.; Iqbal, F.; Khan, M. W.; Mustafa, G.; Mahmood, A.; Mahmood, N.; Shu, X. Bioinspired Synthesis of Zinc Oxide Nano-Flowers: A Surface Enhanced Antibacterial and Harvesting Efficiency. *Mater. Sci. Eng. C* **2020**, *119*, 111280.

(25) Saif, M. S.; Zafar, A.; Waqas, M.; Hassan, S. G.; Haq, A.; Tariq, T.; Batool, S.; Dilshad, M.; Hasan, M.; Shu, X. Phyto-Reflexive Zinc Oxide Nano-Flowers Synthesis: An Advanced Photocatalytic Degra-dation and Infectious Therapy. *J. Mater. Res. Technol.* **2021**, *13*, 2375−2391.

(26) Munawar, T.; Nadeem, M. S.; Mukhtar, F.; Hasan, M.; Mahmood, K.; Arshad, M. I.; Hussain, A.; Ali, A.; Saif, M. S.; Iqbal, F. Rare Earth Metal Co-Doped Zn0·9La0.05M0.05O (M = Yb, Sm, Nd) Nanocrystals; Energy Gap Tailoring, Structural, Photocatalytic and Antibacterial Studies. *Mater. Sci. Semicond. Process.* **2021**, *122*, 105485.

(27) Munawar, T.; Yasmeen, S.; Mukhtar, F.; Nadeem, M. S.; Mahmood, K.; Saif, M. S.; Hasan, M.; Ali, A.; Hussain, F.; Iqbal, F. Zn0.9Ce0.05M0.05O (M = Er, Y, V) Nanocrystals: Structural and Energy Bandgap Engineering of ZnO for Enhancing Photocatalytic and Antibacterial Activity. *Ceram. Int.* **2020**, *46*, 14369−14383.

(28) del Pilar Chantada-Vázquez, M.; López, A. C.; Bravo, S. B.; Vázquez-Estévez, S.; Acea-Nebril, B.; Núñez, C. Proteomic Analysis of the Bio-Corona Formed on the Surface of (Au, Ag, Pt)-Nanoparticles in Human Serum. *Colloids Surf., B* **2019**, *177*, 141−148.

(29) Kobos, L. M.; Adamson, S. X. F.; Evans, S.; Gavin, T. P.; Shannahan, J. H. Altered Formation of the Iron Oxide Nanoparticle-Biocorona Due to Individual Variability and Exercise. *Environ. Toxicol. Pharmacol.* **2018**, *62*, 215−226.

(30) Doumandji, Z.; Safar, R.; Lovera-Leroux, M.; Nahle, S.; Cassidy, H.; Matallanas, D.; Rihn, B.; Ferrari, L.; Joubert, O. Protein and Lipid Homeostasis Altered in Rat Macrophages after Exposure to Metallic Oxide Nanoparticles. *Cell Biol. Toxicol.* **2020**, *36*, 65−82.

(31) Tenzer, S.; Docter, D.; Kuharev, J.; Musyanovych, A.; Fetz, V.; Hecht, R.; Schlenk, F.; Fischer, D.; Kiouptsi, K.; Reinhardt, C.; Landfester, K.; Schild, H.; Maskos, M.; Knauer, S. K.; Stauber, R. H. Rapid Formation of Plasma Protein Corona Critically Affects Nanoparticle Pathophysiology. *Nat. Nanotechnol.* **2013**, *8*, 772−781.

(32) García-álvarez, R.; Vallet-Regí, M. Hard and Soft Protein Corona of Nanomaterials: Analysis and Relevance. *Nanomaterials* **2021**, *11*, 888.

(33) Strojan, K.; Leonardi, A.; Bregar, V. B.; Križaj, I.; Svete, J.; Pavlin, M. Dispersion of Nanoparticles in Different Media Importantly Determines the Composition of Their Protein Corona. *PLoS One* **2017**, *12*, No. e0169552.

(34) Saleh, D. A.; Shimoni, O.; Sosnik, A. Novel Core-Corona Hybrid Nanomaterials Based on the Conjugation of Amphiphilic Polymeric Diblocks to the Surface of Multifunctional Nanodiamond Anchors. *Mater. Today Chem.* **2017**, *3*, 15−26.

(35) Canadian Cancer Statistics Advisory Committee. *Canadian Cancer Statistics 2021*; Canadian Cancer Society, Statistics Canada and the Public Health Agency of Canada, 2021.

(36) Sampathkumar, K.; Riyajan, S.; Tan, C. K.; Demokritou, P.; Chudapongse, N.; Loo, S. C. J. Small-Intestine-Specific Delivery of Antidiabetic Extracts from Withania Coagulans Using Polysaccharide-Based Enteric-Coated Nanoparticles. *ACS Omega* **2019**, *4*, 12049−12057.

(37) Khan, M. I.; Maqsood, M.; Saeed, R. A.; Alam, A.; Sahar, A.; Kieliszek, M.; Miecznikowski, A.; Muzammil, H. S.; Aadil, R. M. Phytochemistry, Food Application, and Therapeutic Potential of the Medicinal Plant (Withania Coagulans): A Review. *Molecules* **2021**, *26*, 6881.

(38) Mbye, M.; Mohamed, H.; Raziq, A.; Kamal-Eldin, A. The Effects of Camel Chymosin and Withania Coagulans Extract on Camel and Bovine Milk Cheeses. *Sci. Rep.* **2021**, *11*, 13573.

(39) Hasan, M.; Zafar, A.; Shahzadi, I.; Luo, F.; Hassan, S. G.; Tariq, T.; Zehra, S.; Munawar, T.; Iqbal, F.; Shu, X. Fractionation of Biomolecules in Withania Coagulans Extract for Bioreductive Nanoparticle Synthesis, Antifungal and Biofilm Activity. *Molecules* **2020**, *25*, 3478.

(40) Asoufi, H. M.; Al-Antary, T. M.; Awwad, A. M. Green Route for Synthesis Hematite (α-Fe2O3) Nanoparticles: Toxicity Effect on the Green Peach Aphid, Myzus Persicae (Sulzer). *Environ. Nanotechnol. Monit. Manag.* **2018**, *9*, 107−111.

(41) Lassoued, A.; Dkhil, B.; Gadri, A.; Ammar, S. Control of the Shape and Size of Iron Oxide (α-Fe2O3) Nanoparticles Synthesized through the Chemical Precipitation Method. *Results Phys.* **2017**, *7*, 3007−3015.

(42) Qasim, S.; Zafar, A.; Saif, M. S.; Ali, Z.; Nazar, M.; Waqas, M.; Haq, A. U.; Tariq, T.; Hassan, S. G.; Iqbal, F.; Shu, X.-G.; Hasan, M. Green Synthesis of Iron Oxide Nanorods Using Withania Coagulans Extract Improved Photocatalytic Degradation and Antimicrobial Activity. *J. Photochem. Photobiol., B* **2020**, *204*, 111784.

(43) Geho, D. H.; Jones, C. D.; Petricoin, E. F.; Liotta, L. A. Nanoparticles: Potential Biomarker Harvesters. *Curr. Opin. Chem. Biol.* **2006**, *10*, 56−61.

(44) Lala, S. Nanoparticles as Elicitors and Harvesters of Economically Important Secondary Metabolites in Higher Plants: A Review. *IET Nanobiotechnol.* **2021**, *15*, 28−57.

(45) Capomaccio, R.; Osório, I.; Ojea-Jiménez, I.; Ceccone, G.; Colpo, P.; Gilliland, D.; Hussain, R.; Siligardi, G.; Rossi, F.; Ricard-Blum, S.; Calzolai, L. Gold Nanoparticles Increases UV and Thermal Stability of Human Serum Albumin. *Biointerphases* **2016**, *11*, 04B310.

(46) Pant, M. P.; Mariam, J.; Joshi, A.; Dongre, P. M. UV Radiation Sensitivity of Bovine Serum Albumin Bound to Silver Nanoparticles. *J. Radiat. Res. Appl. Sci.* **2014**, *7*, 399−405.

(47) Moraru, C.; Mincea, M.; Menghiu, G.; Ostafe, V. Under-standing the Factors Influencing Chitosan-Based Nanoparticles-

Protein Corona Interaction and Drug Delivery Applications. *Molecules* **2020**, *25*, 4758.

(48) Tomak, A.; Cesmeli, S.; Hanoglu, B. D.; Winkler, D.; Oksel Karakus, C. Nanoparticle-Protein Corona Complex: Understanding Multiple Interactions between Environmental Factors, Corona Formation, and Biological Activity. *Nanotoxicology* **2021**, *15*, 1331−1357.

(49) Ban, Z.; Yuan, P.; Yu, F.; Peng, T.; Zhou, Q.; Hu, X. Machine Learning Predicts the Functional Composition of the Protein Corona and the Cellular Recognition of Nanoparticles. *Proc. Natl. Acad. Sci. U. S. A.* **2020**, *117*, 10492−10499.

(50) Alberg, I.; Kramer, S.; Schinnerer, M.; Hu, Q.; Seidl, C.; Leps, C.; Drude, N.; Möckel, D.; Rijcken, C.; Lammers, T.; Diken, M.; Maskos, M.; Morsbach, S.; Landfester, K.; Tenzer, S.; Barz, M.; Zentel, R. Polymeric Nanoparticles with Neglectable Protein Corona. *Small* **2020**, *16*, 1907574.

(51) Luo, F.; Zeng, D.; Chen, R.; Zafar, A.; Weng, L.; Wang, W.; Tian, Y.; Hasan, M.; Shu, X. PEGylated Dihydromyricetin-Loaded Nanoliposomes Coated with Tea Saponin Inhibit Bacterial Oxidative Respiration and Energy Metabolism. *Food Funct.* **2021**, *12*, 9007−9017.

(52) Huang, L.; Chen, R.; Luo, J.; Hasan, M.; Shu, X. Synthesis of Phytonic Silver Nanoparticles as Bacterial and ATP Energy Silencer. *J. Inorg. Biochem.* **2022**, *231*, 111802.

(53) Luo, D.; Zhan, S.; Xia, W.; Huang, L.; Ge, W.; Wang, T. Proteomics Study of Serum Exosomes from Papillary Thyroid Cancer Patients. *Endocr. Relat. Cancer* **2018**, *25*, 879−891.

(54) Lim, L. C.; Looi, M. L.; Zakaria, S. Z. S.; Sagap, I.; Rose, I. M.; Chin, S. F.; Jamal, R. Identification of Differentially Expressed Proteins in the Serum of Colorectal Cancer Patients Using 2D-DIGE Proteomics Analysis. *Pathol. Oncol. Res.* **2016**, *22*, 169−177.

(55) Zhong, M. E.; Chen, Y.; Xiao, Y.; Xu, L.; Zhang, G.; Lu, J.; Qiu, H.; Ge, W.; Wu, B. Serum Extracellular Vesicles Contain SPARC and LRG1 as Biomarkers of Colon Cancer and Differ by Tumour Primary Location. *EBioMedicine* **2019**, *50*, 211−223.

(56) Cima, I.; Schiess, R.; Wild, P.; Kaelin, M.; Schüffler, P.; Lange, V.; Picotti, P.; Ossola, R.; Templeton, A.; Schubert, O.; Fuchs, T.; Leippold, T.; Wyler, S.; Zehetner, J.; Jochum, W.; Buhmann, J.; Cerny, T.; Moch, H.; Gillessen, S.; Aebersold, R.; Krek, W. Cancer Genetics-Guided Discovery of Serum Biomarker Signatures for Diagnosis and Prognosis of Prostate Cancer. *Proc. Natl. Acad. Sci. U. S. A.* **2011**, *108*, 3342−3347.

(57) Sinha, A.; Hussain, A.; Ignatchenko, V.; Ignatchenko, A.; Tang, K. H.; Ho, V. W. H.; Neel, B. G.; Clarke, B.; Bernardini, M. Q.; Ailles, L.; Kislinger, T. N-Glycoproteomics of Patient-Derived Xenografts: A Strategy to Discover Tumor-Associated Proteins in High-Grade Serous Ovarian Cancer. *Cell Syst.* **2019**, *8*, 345−351.

(58) Tyanova, S.; Cox, J. P. A Bioinformatics Platform for Integrative Analysis of Proteomics Data in Cancer Research. *Methods Mol. Biol.* **2018**, *1711*, 133−148.

(59) Shi, Y.; Zhai, H.; Wang, X.; Han, Z.; Liu, C.; Lan, M.; Du, J.; Guo, C.; Zhang, Y.; Wu, K.; Fan, D. Ribosomal Proteins S13 and L23 Promote Multidrug Resistance in Gastric Cancer Cells by Suppressing Drug-Induced Apoptosis. *Exp. Cell Res.* **2004**, *296*, 337−346.

(60) Freeman, A. K.; Morrison, D. K. 14-3-3 Proteins: Diverse Functions in Cell Proliferation and Cancer Progression. *Semin. Cell Dev. Biol.* **2011**, *22*, 681−687.

(61) Jin, L.; Huo, Y.; Zheng, Z.; Jiang, X.; Deng, H.; Chen, Y.; Lian, Q.; Ge, R.; Deng, H. Down-Regulation of Ras-Related Protein Rab 5C-Dependent Endocytosis and Glycolysis in Cisplatin-Resistant Ovarian Cancer Cell Lines. *Mol. Cell. Proteomics* **2014**, *13*, 3138−3151.

(62) Zhou, G.; Zhang, H.; Lin, A.; Wu, Z.; Li, T.; Zhang, X.; Chen, H.; Lu, D. Multi-Omics Analysis in *β*-Thalassemia Using an HBB Gene-Knockout Human Erythroid Progenitor Cell Model. *Int. J. Mol. Sci.* **2022**, *23*, 2807.

(63) Kim, T. H.; Koo, J. H.; Heo, M. J.; Han, C. Y.; Kim, Y. I.; Park, S. Y.; Cho, I. J.; Lee, C. H.; Choi, C. S.; Lee, J. W.; Kim, W.; Cho, J. Y.; Kim, S. G. Overproduction of Inter-a-Trypsin Inhibitor Heavy Chain 1 after Loss of Ga13 in Liver Exacerbates Systemic Insulin Resistance in Mice. *Sci. Transl. Med.* **2019**, *11*, 4735.

(64) Smith, M. D.; Harley, M. E.; Kemp, A. J.; Wills, J.; Lee, M.; Arends, M.; von Kriegsheim, A.; Behrends, C.; Wilkinson, S. CCPG1 Is a Non-Canonical Autophagy Cargo Receptor Essential for ER-Phagy and Pancreatic ER Proteostasis. *Dev. Cell* **2018**, *44*, 217−232.

(65) Shimada, K.; Uzawa, K.; Kato, M.; Endo, Y.; Shiiba, M.; Bukawa, H.; Yokoe, H.; Seki, N.; Tanzawa, H. Aberrant Expression of RAB1A in Human Tongue Cancer. *Br. J. Cancer* **2005**, *92*, 1915−1921.

(66) Albakova, Z.; Siam, M. K. S.; Sacitharan, P. K.; Ziganshin, R. H.; Ryazantsev, D. Y.; Sapozhnikov, A. M. Extracellular Heat Shock Proteins and Cancer: New Perspectives. *Transl. Oncol.* **2021**, *14*, 100995.

(67) Kabir, M. M.; Ho, Y. H.; Shimizu, K. Effect of LdhA Gene Deletion on the Metabolism of Escherichia Coli Based on Gene Expression, Enzyme Activities, Intracellular Metabolite Concentrations, and Metabolic Flux Distribution. *Biochem. Eng. J.* **2005**, *26*, 1−11.

(68) Xu, Y.; Wu, W.; Han, Q.; Wang, Y.; Li, C.; Zhang, P.; Xu, H. New Insights into the Interplay between Non-Coding RNAs and RNA-Binding Protein HnRNPK in Regulating Cellular Functions. *Cells* **2019**, *8*, 62.

(69) Iqbal, J.; Li, W.; Hasan, M.; Juan Li, Y.; Ullah, K.; Yun, W.; Awan, U.; Qing, H.; Deng, Y. Distortion of Homeostatic Signaling Proteins by Simulated Microgravity in Rat Hypothalamus: A16O/18O-Labeled Comparative Integrated Proteomic Approach. *Proteomics* **2014**, *14*, 262−273.

(70) Iqbal, J.; Li, W.; Ullah, K.; Hasan, M.; Linna, G.; Awan, U.; Zhang, Y.; Batool, S.; Qing, H.; Deng, Y. Study of Rat Hypothalamic Proteome by HPLC/ESI Ion Trap and HPLC/ESI-Q-TOF MS. *Proteomics* **2013**, *13*, 2455−2468.

(71) Iqbal, J.; Li, W.; Hasan, M.; Liu, K.; Awan, U.; Saeed, Y.; Zhang, Y.; Muhammad Khan, A.; Shah, A.; Qing, H.; Deng, Y. Differential Expression of Specific Cellular Defense Proteins in Rat Hypothalamus under Simulated Microgravity Induced Conditions: Comparative Proteomics. *Proteomics* **2014**, *14*, 1424−1433.

(72) Cantalapiedra, C. P.; Hernández-Plaza, A.; Letunic, I.; Bork, P.; Huerta-Cepas, J. EggNOG-Mapper v2: Functional Annotation, Orthology Assignments, and Domain Prediction at the Metagenomic Scale. *Mol. Biol. Evol.* **2021**, *38*, 5825−5829.

(73) Chen, C.; Chen, H.; He, Y.; Xia, R. TBtools, a Toolkit for Biologists Integrating Various Biological Data Handling Tools with a User-Friendly Interface. *bioRxiv* **2018**, *13*, 1194−1202.

(74) Lu, S.; Wang, J.; Chitsaz, F.; Derbyshire, M. K.; Geer, R. C.; Gonzales, N. R.; Gwadz, M.; Hurwitz, D. I.; Marchler, G. H.; Song, J. S.; Thanki, N.; Yamashita, R. A.; Yang, M.; Zhang, D.; Zheng, C.; Lanczycki, C. J.; Marchler-Bauer, A. CDD/SPARCLE: The Conserved Domain Database in 2020. *Nucleic Acids Res.* **2020**, *48*, D265−D268.

(75) Bailey, T. L.; Johnson, J.; Grant, C. E.; Noble, W. S. The MEME Suite. *Nucleic Acids Res.* **2015**, *43*, W39−W49.